Pillar[5]arene-Derived endo-Functionalized Molecular Tube for Mimicking Protein-Ligand Interactions

Ke Wen (wenk@sari.ac.cn)
Shanghai Advance Research Institute, Chines Academy of Sciences
Zhuo Wang
Shanghai Advance Research Institute, Chines Academy of Sciences
Tao Chen
Shanghai Advance Research Institute, Chines Academy of Sciences https://orcid.org/0000-0001-6110-9112
Hua Liu
ShanghaiTech University
Yahu Liu
ChemBridge Research Laboratories
Xiao-Li Zhao
East China Normal University
Wei-Bo Hu
Shanghai Advance Research Institute, Chines Academy of Sciences
Hui Yang
Shanghai Advanced Research Institute, Chinese Academy of Sciences

Article

Keywords:

Posted Date: January 13th, 2021

DOI: https://doi.org/10.21203/rs.3.rs-145539/v1

Abstract

Artificial tubular molecular pockets bearing polar functionalities on their inner surface are useful model systems for understanding the mechanisms of protein-ligand interactions in living systems. We herein report a pillar[5]arene-derived molecular tube, [P4-(OH)BPO], whose endo conformational isomer endo-[P4-(OH)BPO] possesses an inwardly pointing hydrogen-bond (H-bond) donor (OH) in its deep cavity, a strong H-bond acceptor (C=O) on the predominantly hydrophobic inner surface, rendering it a perfect protein binding pocket mimetic. By measuring the binding affinity of this pocket-mimetic tube, we screened a library of various shape-complementary organic guests (1–38) resembling the fragment ligands in fragment-based drug design (FBDD). On the basis of the data for "fragment-pocket" complexes (1–38)⊂endo-[P4-(OH)BPO], two rationally designed "lead molecules" (39 and 40) were identified to be able to enhance binding affinity significantly by forming H-bonds with both the donor and acceptor of endo-[P4-(OH)BPO]. The described work opens new avenues for developing pillar[n]arene-derived protein binding pocket-mimetic systems for studies on protein-ligand interactions and mechanisms of enzymatic reactions.

Introduction

Small molecules are the most common modality for new medicines, accounting for 67% of the FDA-approved drugs in 2019[1]. Almost all current small-molecule drugs act by targeting disease-related proteins in the human body and regulating their activity[2,3]. As the interaction between a protein and a small molecule is often through binding of the molecule in a pocket on the protein surface, characterization of such binding pockets is important to elucidate the disease mechanisms and design new drug molecules[4-6]. Along with various methods, model studies using biomimetic receptors – artificially fabricated functional macrocyclic hosts – to mimic protein binding pockets are useful for understanding the nature of protein-ligand recognition[7,8]. During the past decades, the approach of fragment-based drug design (FBDD) has attracted increasing interest both in academia and pharmaceutical industry[9-10]. In FBDD, drug compounds were designed on the basis of protein-ligand bonding using fragment ligands with low complexity in chemical structures and low molecular weights[9-10]. It is well established that a protein binding pocket has an interior surface bearing both polar and non-polar functionalities for synergistic hydrogen bonding and hydrophobic interactions with a guest molecule[4-5]. In a reported survey of fragment-pocket complexes, hydrogen bonds (H-bonds) stabilize 89% of the fragment-pocket complexes, with 74% of the entries displaying one to three H-bonds[10]. Therefore, in order to imitate the microenvironment within protein binding pockets, the interior surface of the biomimetic receptors must possess polar functionalities for H-bond formation. To this end, there have been reports on pocket-shaped receptors, such as cavitands[11], glucose receptor 2[12], aryl-extended calix[4]pyrrole receptors[13], helical aromatic and oligoamide foldamers (Fig. 1a-e) [14,15]. Jiang's group recently made significant progress in transforming naphthalene-based tubular molecules into biomimetic tubes in which the inwardly directed functional groups improved their binding affinity and selectivity

toward fragment ligands (Fig. 1f)[16–18]. As a class of tubular-shaped macrocyclic hosts, pillar[n]arenes[19-21] could seat various functional substituents on their rims, for instance, amino acids or short peptides, for mimicking transmembrane channels[22]. Nonetheless, all of these rim-embedded polar functional substituents pointed outwards, and there has been no report on mounting polar functionalities pointing inwardly to the cavity cores of pillar[n]arenes. Herein, we report the creation of a pillar[5]arene-derived tubular molecular pocket with an inward-pointing hydroxyl group, endo-**[P4-(OH)BPO]** (Fig. 1g), which could unidirectionally interact with various small shape-complementary polar molecular guests through synergistic hydrophobic and hydrogen bonding interactions within its tubular cavity, mimicking a fragment-pocket in FBDD or protein-ligand interaction event in a protein binding pocket.

Results And Discussion

Formation of endo-**[P4-(OH)BPO].** Our group has previously developed unique methods to grow functional substituents on the rims of pillar[n]arenes[23]. We conjectured that a pillar[n]arene-derived protein binding pocket mimetic could be realized through mounting a polar functionality on the rim of a pillar[n]arene, and then forcing it to point towards the tubular core either through steric effect or substrate-induced conformational change. We therefore started our work from adding a small polar functionality, hydroxyl group, to the rim of pillar[5]arene by creating a quaternary carbon atom through a nucleophilic addition reaction of pillar[4]arene[1]quinone (**P4Q**) with phenylmagnesium chloride (or phenyllithium) (Supplementary Information). The resultant product, pillar[4]arene[1]1-hydroxy-[1,1'-biphenyl]-4(1H)-one (**[P4-(OH)BPO]**), was characterized by ^{1}H and ^{13}C NMR spectroscopy, atmospheric pressure chemical ionization mass spectroscopy (APCI-MS), and single crystal X-ray diffraction analysis (Supplementary Information). The X-ray crystallography data of a single crystal obtained by slow evaporation of a solution of [**P4-BPO(1-OH**)] in acetone (Fig. 2a) clearly showed that (**[P4-(OH)BPO]**) has its phenyl group positioned outside the tubular frame, and its hydroxyl group pointing towards the core of the cavity, with an acetone molecule encapsulated inside the cavity through formation of a H-bond between the C=O group of acetone and the O–H group of **[P4-(OH)BPO]**, which is a unambiguous evidence of the adoption of an endo conformational isomer, endo-**[P4-(OH)BPO]**.

endo-[P4-(OH)BPO] as protein binding pocket mimetic. FBDD is an approach to develop potent small-molecule compounds starting from fragments binding weakly to target proteins[9,10]. Owing to its advantages such as saving experimental cost, offering diverse hits, and exhibiting multiple ways of binding, FBDD has been playing important roles in target-based drug discovery. In FBDD, fragment ligands are usually small molecules with low complexity in chemical structure, and H-bonds play an important role in stabilizing the fragment-pocket complexes[9-10]. For example, among the 462 unique fragment-pocket complexes investigated by Giordanetto, Shaw and co-workers, 92% of the fragments have at least one hydrogen bond formed with a protein, a structural water molecule, or a metal atom[10]. Given the role of H-bonds in fragment-pocket complexes, endo-**[P4-(OH)BPO]**, with an inwardly pointing H-bond donor (-OH) at the bottom of its deep cavity, a strong H-bond acceptor (C=O) on the tubular inner wall of a predominantly hydrophobic surface, is naturally an appealing artificial protein binding pocket.

Binding of fragments to endo-[P4-(OH)BPO]. Recently, several biomimetic pockets with polar binding sites in their hydrophobic pockets have been disclosed[11-18]. Impressively, thermodynamics of interactions between biomimetic pockets and guests in water has been studied systematically by Jiang and co-workers[16-18], which is highly valuable as the recognizations of ligands by protein binding pockets occur in aqueous environment in living systems. However, it is challenging to assess the contribution to pocket-ligand binding affinity "solely" from hydrogen bonding only through studies on the complexation in water. The reasons include: a) water molecules intend to bind the inner polar site of a synthetic receptor, and b) water molecules compete with a host in binding with a polar guest, weakening H-bond interaction between the host and guest[16-18]. In order to better understand both big picture and details of molecular recognition, investigation of pocket-fragment complexation in non-polar environment should be indispensably complimentary to the studies in aqueous solutions. Therefore, we initiated a thermodynamic study on the fragment-pocket binding abilities and selectivities of endo-**[P4-(OH)BPO]** with respect to various guest compounds in a non-polar solvent, $CDCl_3$. In selecting guests for the study, ideal guest compounds resembling "fragment ligands" in FBDD are those not only geometrically complementary to the tubular binding pocket, but, more importantly, bearing H-bond acceptor(s) or donor(s) or both so that such a host-guest interaction could mimic a protein-ligand interaction event staged synergistically by both hydrogen bonding and hydrophobic interaction[9,10]. We selected an array of small-molecule fragment compounds for a "fragment library" which includes alkyl amines, alcohols, aldehydes, acids, esters, small heterocycles, and simple small molecules possessing bilogically important functional groups (Fig. 3). ^{1}H NMR experiments were performed on all of the host-guest pairs at 1:1 ratio in $CDCl_3$ (Supplementary Information). The shifts of the proton signals of the complexed guests relative to the free species were used to evaluate the binding events. The binding constants (K_a) and binding free energies were determined by the ^{1}H NMR titration method (Table 1)[24]. Generally, the energy of a single H-bond is somewhat between a van der Waals interaction and a fully covalent or ionic bond, but it varies depending on the nature of the donor and acceptor atoms, their geometries, and surrounding environments[25,26]. Thus, the "fragment-pocket" interaction of **[P4-(OH)BPO]** with a guest was expected to be affected by the number of H-bonds, angles of the hydrogen bond(s), nature of the donor and acceptor atoms, and the hydrophobic interaction between the inner surface of endo-**[P4-(OH)BPO]** and the guest[25,26]. In order to explore the correlations of the binding strength (K_a) and properties of guest fragments, molecular descriptors including the logarithm of the octanol:water partition coefficient (log P), dipole moment (μ), molecular volume (V), surface area (S), and asphericity Ω_a) were collected[16,27].

Table 1. Fragment library compounds screened in fragment-pocket complexation

compound	K_a (M^{-1})[a]	R^2	- ΔG[b]	V ($Å^3$)[c]	Ω_a[d]	S ($Å^2$)[e]	log P[f]	μ(D)[g]
1	138.0±20.7	0.9957	11.8-12.6	129.80	0.18040	141.48	0.86	1.159
2	92.7±11.0	0.9942	10.9-11.5	177.01	0.21016	183.71	2.06	1.143
3	42.0±6.3	0.9880	8.9-9.6	224.21	0.22452	225.94	2.90	1.139
4	67.4±13.1	0.9977	9.9-10.9	123.07	0.18229	136.00	0.84	2.057
5	24.0±2.1	0.9936	7.7-8.1	170.27	0.21121	178.24	2.03	2.038
6	28.0±2.6	0.9941	8.0-8.5	217.47	0.22514	220.47	3.07	2.020
7	40.8±13.0	0.9957	8.2-9.9	115.11	0.18099	129.54	0.88	3.490
8	24.1±3.5	0.9987	7.5-8.2	162.30	0.20842	171.83	1.78	3.593
9	10.6±1.6	0.9998	5.4-6.2	209.51	0.22311	214.08	2.95	3.640
10	11.2±1.6	0.9989	5.6-6.3	147.78	0.16638	159.66	1.30	5.115
11	8.8±1.8	0.9987	4.8-5.9	195.01	0.20433	201.95	2.31	5.080
12	1.7±0.1	0.9996	1.2-1.5	242.19	0.22186	244.18	3.33	4.805
13	8.7±0.3	0.9992	5.3-5.4	123.99	0.13045	137.19	0.79	5.097
14	5.2±0.3	0.9982	3.9-4.2	171.15	0.19348	179.29	1.92	4.940
15	3.3±0.2	0.9989	2.8-3.1	218.36	0.21638	221.53	3.05	4.949
16	321.6±17.0	0.9999	14.2-14.4	83.08	0.11042	100.38	-2.06	4.853
17	22.5±2.2	0.9992	7.5-7.9	106.69	0.08171	120.67	-1.01	4.685
18	390.5±75.9	0.9957	14.3-15.2	106.79	0.08234	120.75	-1.55	4.961
19	241.5±22.9	0.9993	13.4-13.8	248.40	0.21017	247.71	1.50	5.259
20	109.4±16.1	0.9981	11.2-12.0	106.44	0.09492	121.96	-0.70	4.786
21	222.9±32.0	0.9985	13.0-13.7	130.15	0.13194	143.33	-0.19	4.391
22	103.9±3.6	0.9992	11.4-11.6	153.76	0.14146	163.59	0.32	4.446
23	58.6±3.2	0.9957	10.0-10.2	177.36	0.15542	184.78	0.83	4.412
24	123.5±13.6	0.9961	11.7-12.2	129.62	0.13367	142.39	-0.19	4.559
25	67.3±2.8	0.9955	10.3-10.5	247.79	0.17616	247.68	2.36	4.149
26	4.7±0.2	0.9993	3.7-3.9	138.11	0.05565	146.37	-0.64	4.631
27	nd[h]			107.72	0.04061	119.30	0.46	2.470
28	nd[h]			85.86	0.06253	99.95	0.75	3.745
29	83.0±15.1	0.9963	10.5-11.4	95.76	0.06253	106.64	-0.08	1.918
30	6.4±0.4	0.9987	4.4-4.8	90.78	0.06253	106.64	0.05	4.139
31	11.2±1.6	0.9989	5.6-6.3	101.33	0.07198	111.92	0.44	1.517

32	13.8±2.3	0.9989	6.1-6.9	124.95	0.10538	133.83	0.97	1.263
33	11.2±1.6	0.9989	5.6-6.3	136.16	0.12523	144.96	1.43	3.910
34	11.2±1.6	0.9989	5.6-6.3	185.70	0.16779	189.26	1.43	4.908
35	101.5±14.6	0.9983	11.1-11.8	102.60	0.03071	116.00	-1.35	5.552
36	52.4±9.0	0.9972	9.3-10.2	118.43	0.13632	132.34	0.87	4.572
37	28.6±3.2	0.9990	8.0-8.6	66.25	0.21003	84.87	-0.34	4.123
38	11.2±1.6	0.9989	5.6-6.3	159.13	0.18420	167.76	1.86	2.828
39	750.1±31.5	0.9999	16.3-16.5	163.20	0.15823	173.05	-1.31	2.743
40	1190±89.5	0.9999	17.4-17.7	139.89	0.14959	151.57	-2.52	6.032

[a]Experiments were performed in $CDCl_3$ at 298K (Supplementary Information). [b]$\Delta G = -RT\ln K_a$. [c]Calculated based on optimized structures. [d]Calculated by the principal moments of inertia of guests. [e]Calculated by using Multiwfn program[28]. [f]Values were taken from references[16,29,30]. [g]Calculated with Gaussian 09 at the RB3LYP/6-31++G level of calcualtions[31]. [h]Values were too small to be determined.

Fragment-pocket complexation. We first assessed the binding between **[P4-(OH)BPO]** and fragments including alkyl amines, alcohols, aldehydes, acids, and esters (Table 1). The formation of fragment-pocket complexes between **[P4-(OH)BPO]** and the guests was evidenced by obvious upfield shifting of the proton signals of *a*-carbons of the guests (**1-15**) in the ^{1}H NMR spectra of the fragment-pocket pairs in a 1:1 molar ratio in non-polar solvent. As shown in the ^{1}H NMR spectra (Fig. 4), upon mixing *n*-butyric acid (**13**) and **[P4-BPO(1-OH)]** in $CDCl_3$, obvious upfield shifts for the methylene ($\Delta\delta_\alpha$ = -0.26 ppm and $\Delta\delta_\beta$ = -0.25 ppm) and the terminal methyl ($\Delta\delta_\gamma$ = -0.14 ppm) proton signals of **13** were observed. In addition, NOE correlations between protons (H*a*) of **13** and the 1,4-dimethoxybenzene protons of **[P4-BPO(1-OH)]** were observed in the 2D NOESY spectrum (Supplementary Fig. S170). The ^{1}H NMR and 2D NOESY data, together with Job plot (Supplementary Fig. S60) and APCI mass spectrum (peak *m/z* = 893.4014 for (**13⊂[P4-BPO(1-OH)] + Li**)$^+$ (Supplementary Fig. S18), proved the formation of a 1:1 complex **13⊂[P4-BPO(1-OH)]**. Similarly, alkyl amines (**1**–**3**) and alcohols (**4**–**6**) formed fragment-pocket complexes **G⊂[P4-BPO(1-OH)]** (**G** = **1**–**6**) with binding constants ranging from 40 to 140 M^{-1} and from 30 to 70 M^{-1}, respectively. The binding constants between **[P4-BPO(1-OH)]** and aldehydes (**7-9**), esters (**10-12**) and acids (**13-15**) were smaller compared with those of amines (**1-3**) and alcohols (**4-6**). The large binding constants between the host and fragments **1**-**6** reflected stronger binding interaction originated from the H-bond accepting ability of the nitrogen atom of aliphatic amines or the oxygen atom of aliphatic alcohol[32-34]. As previously described by Smulders, Zarra and Nitschke[27], higher μ and lower log *P* values meant more polarity of guests. Thus, it was not surprising to see that higher binding affinities correlate to higher μ and lower log *P* values in the cases of complexation in non-polar solvent $CDCl_3$. Polar compounds tend to escape from non-polar solvent, and clutch H-bond donor in the deep pockets, which

could explain the correlations between experimental values (K_a and ΔG) and calculated values (μ and log *P*) demonstrated by the guests **1**-**25** in the Table 1.

With the formation of fragment-pocket complexes confirmed, we wondered whether the host was in its *endo* conformation where the inward-pointing OH group forms a H-bond with a guest. Unambiguous evidence of *endo* conformation of **[P4-BPO(1-OH)]** in the complex was obtained from the X-ray diffraction analysis. The single crystal structure of the complex **13**⊂*endo*-**[P4-BPO(1-OH)]** (Fig. 2c) revealed that **13** is encapsulated in the host pocket with its alkyl chain in the hydrophobic tubular region of the host cavity, and, unmistakably, with its carbonyl oxygen H-bonded to the inwardly pointing OH group in the deep cavity of the host, with the CO···HO distance of 1.941 Å, perfectly in the range of a typical H-bond length[35]. Thus, the complex **13**⊂*endo*-**[P4-BPO(1-OH)]** is synergistically stabilized by both hydrogen bonding and hydrophobic interactions. We also obtained crystal structures of a few representative fragment-pocket complexes **G**⊂*endo*-**[P4-BPO(1-OH)]** (**G = 9, 17, 21, 24, 25, 31,** and **35**) in which the carbonyl oxygen is bonded to the OH group of *endo*-**[P4-BPO(1-OH)]** in the deep pocket (Fig. 2b, 2d-i). Consequently, we could deduce that in the fragment-pocket complexes **1-25**⊂**[P4-BPO(1-OH)]**, **[P4-BPO(1-OH)]** was in an *endo* conformation with its OH group inwardly pointing to interact with H-bond acceptor of a guest fragment.

Amides are commonly seen in drug molecules[36]. Amide functional groups have weak basic and acidic possibilities[37]. The role of a H-bond between an amide guest and the hydroxyl of **[P4-(OH)BPO]** in stabilizing a fragment-pocket complex is significant[37], which was reflected in our model fragment-pocket binding study: Complexes **G**⊂*endo*-**[P4-(OH)BPO]** (**G** = **16**–**25**, Table 1) were found to have much larger K_a values than **G**⊂*endo*-**[P4-(OH)BPO]** (**G** = **1**–**15**, **26**–**38**, Table 1). Besides H-bonding, hydrophobic interaction also plays a significant role in stabilizing the fragment-pocket complexes in which the hydrophobic fragments of the ligands are energetically favored at the interface of the host pocket[38,39] Thus, the binding mode of an amide fragment in a “fragment-pocket” complex is determined not only by the strength of amide carbonyl-hydroxyl (CO···HO) H-bond, but also by the hydrophobic interaction between the inner cavity of the host and the guest chain[38,39]. This was well reflected in complexes **21**⊂*endo*-**[P4-(OH)BPO]** and **24**⊂*endo*-**[P4-(OH)BPO]** where alkyl chains of guests **21** and **24** were trapped in the host pocket albeit they were connected to different points of amide functional group (either to the amino N or the carbonyl C atoms, respectively), as shown by the single crystal X-ray structures (Fig. 2e and 2f). The hydrophobic interaction between the *predominantly hydrophobic inner surface* of the pocket and the alkyl chain of the fragment determined the binding modes of these two complexes. As **21** was more polar (higher μ and lower log *P* value) than **24** (Table 1), the K_a value of **21**⊂*endo*-**[P4-(OH)BPO]** doubled that of **24**⊂*endo*-**[P4-(OH)BPO]** (Table 1). As amide **25** has two butyl groups connected to the amino N and the carbonyl C, respectively, two possible binding modes for **25** exist with either of the two butyl groups confined in the cavity of *endo*-**[P4-(OH)BPO]**. The ^{1}H NMR data (Supplementary Fig. S21,) and the crystal structure of **25**⊂*endo*-**[P4-(OH)BPO]** (Fig. 2g) indicated that the amine subgroup of **25** was left outside of the binding pocket, possibly owing to the difference in charge density and polarity between the N and C atoms associated with the C=O (Mulliken charges calculated to be -0.518556e and

-0.417205e for the N and C atoms, respectively) (Supplementary Information). As a consequence, the solvation interaction between the solvent-exposed N-butyl chain and the “nonpolar” solvent ($CDCl_3$) brought down the stability of **25⊂*endo*-[P4-(OH)BPO]**[40], as evidenced by its lower K_a than those of the **21⊂*endo*-[P4-(OH)BPO]** and **24⊂*endo*-[P4-(OH)BPO]**.

Heterocyclic rings are predominant architectural components of pharmaceuticals and allow for variable biological interactions otherwise hard to achieve[41,42]. The binding of five membered heterocycles (**26**-**34**), non-aromatic and aromatic, to *endo*-**[P4-BPO(1-OH)]** were thus studied. The obvious upfield shifts of the proton signals of the five membered heterocyclic guests (**26**-**34**) in the ^{1}H NMR spectra in $CDCl_3$ upon mixing with **[P4-BPO(1-OH)]** evidenced the formation of the corresponding host-guest complexes (Table 1). Unambiguous evidence of an examplar heterocyclic fragment-pocket complex was provided by the single crystal structure of **30⊂*endo*-[P4-BPO(1-OH)]** which revealed that thiazole **30** is cramped in the tubular cavity of *endo*-**[P4-BPO(1-OH)]** with its N atom forming a H-bond with the -OH group of the host (Fig. 2h). Among “screened” heterocyclic fragments, imidazole **29** formed fragment-pocket complex with a higher bonding constant (Table 1), which implied that **29** might use both of its H-bond acceptor (=N) and donor (-NH) in the interaction with the pocket.

Sulfoxide, oxirane, nitrile and nitro group frequently appear in pharmaceuticals[43-47]. We therefore included fragments dimethyl sulfoxide (DMSO) (**35**), 1-nitropropane (**36**), acetonitrile (**37**) and 2-butyloxirane (**38**) in our exploration of fragment-pocket interaction study. DMSO molecule is dipolar aprotic with a strong polar sulfoxide group and two hydrophobic methyl moieties[43,44], which facilitate the formation of a stable complex **35⊂*endo*-[P4-BPO(1-OH)]** (Fig. 2f). With a nitro group that forms H-bond with a -OH group[45], plus a propyl chain to reach the hydrophobic area in the host’s cavity, fragment **36** formed stable **36⊂*endo*-[P4-BPO(1-OH)]** as expected. Nitrile group plays efficacious roles of in drug molecules[46], so acetonitrile (**37**), with simple structure (linear N≡C−C skeleton) and small size (C−N distance 1.16 Å), was selected as a nitrile fragment. The H-bond formed between C≡N nitrogen and -OH of the host was not strong, and the hydrophobic methyl did not contribute much binding affinity, which result in a low binding constant for **37⊂*endo*-[P4-BPO(1-OH)]**. 2-Butyloxirane (**38**) formed **38⊂*endo*-[P4-BPO(1-OH)]** with a low K_a possibly owing to the weak H-bond between OH of the host and the oxirane oxygen[47].

Fragment-based drug design (FBDD). Encouraged by the aforementioned results of the fragment-pocket complexes **G⊂*endo*-[P4-BPO(1-OH)]** (**G** = **1**−**38**), we attempted a model FBDD aiming at “lead molecules” to bind the “target” pocket – *endo*-**[P4-BPO(1-OH)]**. Among the fragments **1**-**38**, amides **16**, **18**, **19** and **21**, with amine alkyl chains, gave binding constants greater than 200 M^{-1}, so these *N*-alkyl substituted formamides and acetamides were designated as the screening-generated “hit molecules”. Given that all of the fragments **1**-**38** are monofunctional, and do not have structural handle to utilize the H-bond acceptors on the inner surface of *endo*-**[P4-BPO(1-OH)]** cavity, bifunctional amides **39** and **40** possessing an H-bond donor at the other end of the molecules were designed for the “target” *endo*-**[P4-BPO(1-OH)]**. We were delighted to see that the binding constants of designed bifunctional “lead molecules” **39** and **40**

were enhanced by more than 13 and 20 folds, respectively, compared to their monofunctional analog **23** (Table 1). We were delighted to see that **40** achieved the highest binding strength among all of the fragments listed in Table 1 with a K_a of 1.2×10^3 [M^{-1}]. The stronger binding of **40** with *endo*-**[P4-BPO(1-OH)]** than that of **39** could be partially explained by the higher diploe moment and lower log *P* of the former than the latter (Table 1). In the ^{1}H NMR spectra of both complexes (Supplementary Fig. S45 and S46), significant upfield shifting of methylene proton signals of the bound guest was observed, implying that the guests were embraced inside the pocket cavity. Despite extensive efforts, crystalization of the fragment-pocket complexes **39** or **40**⊂*endo*-**[P4-BPO(1-OH)]** was not successful. Nonetheless, computational docking of **39** and **40** to the pocket of *endo*-**[P4-BPO(1-OH)]** (Fig. 5) clearly demonstrated that the "lead molecules" were bound to the pocket cavity through a H-bond between amide C=O of the fragment and OH in the deep pocket with O···H distance of 1.573 Å and 1.597 Å, respectively, and, remarkably, the second H-bond between the fragment's OH and carbonyl O on the inner wall of pocket cavity with bond length, 1.955 Å and 1.865 Å respectively (Fig. 5).

Complexation through "induced-fit". It is generally believed that the binding of a ligand to a conformationally free protein is mechanistically *via* "conformational selection", whereby a ligand selectively binds to a form of the protein pocket, or *via* "induced fit", whereby a ligand binds to a predominantly free conformation of a protein, followed by a conformational change of the protein to form a preferred protein-ligand complex[49,50]. Theoretically, the rim-bound hydroxyl group in conformationally free **[P4-(OH)BPO]** should be able to park on either inside or outside the tubular wall to result in *endo*-**[P4-BPO(OH)]** or *exo*-**[P4-BPO(OH)]**[23]. In solution, **[P4-(OH)BPO]** exists in a rapid equilibrium between ***endo*-[P4-(OH)BPO]** and ***exo*-[P4-(OH)BPO]** isomers, as evidenced by the single set of proton signals in its ^{1}H NMR spectra in various deuterated solvents, such as dichloromethane-d_2, chloroform-d_3, acetone-d_6, acetonitrile-d_3, DMF-d_4 and DMSO-d_6 (Supplementary Fig. S4), most probably owing to interconversion between the *endo*- and *exo*-conformational isomers in a rate faster than the NMR timescale. We therefore deduced that formation the fragment-pocket complexes **G**⊂*endo*-**[P4-(OH)BPO]** (**G** = **1**−**40**) could be an "induced fit" process where a fragment guest passing through the host tube clutches the freely moving OH through H-bond interaction, and, as a consequence, freezes conformationally free **[P4-(OH)BPO]** into an *endo*-complex. Based on this assumption, we conjectured that an ***exo*-[P4-(OH)BPO]** conformational isomer could be also "frozen" out by non-polar fragment guest geometrically complementary. As expected, ***exo*-[P4-(OH)BPO]** conformational isomer was "frozen" out by solvent-induced crystallization in hexane, and was confirmed by ^{1}H and 2D NOSEY NMR spectra in $CDCl_3$ (Supplementary Fig. S47 and S175) and unambiguously single crystal X-ray structure (Fig. 6) in which the phenyl group linked to the quaternary carbon atom lands on the inner side of the tubular core, leaving the hydroxyl group pointing outside, a hexane molecule is imprisoned in the tubular cavity through solely hydrophobic interaction (Fig. 6).

Conclusion

In summary, we have fabricated a pillar[5]arene-derived molecular tube **[P4-(OH)BPO]**. With an inwardly pointing hydrogen bond donor (OH) in the deep cavity and a hydrogen bond acceptor (*C=O*) on the inner surface, plus a hydrophobic tubular inner wall, the *endo*-conformational isomer, *endo*-**[P4-BPO(1-OH)]**, renders itself a perfect artificial protein binding pocket. On the basis of the study on the binding behavior of various FBDD "fragment ligands" inside the "pocket" of *endo*-**[P4-(OH)BPO]**, "lead molecules" were rationally designed with their binding constants greatly enhanced compared to the screening-generated "hit moleclues". The further work in this direction could be useful in FBDD and artificial protein-ligand binding models to facilitate our understanding of complex molecular interactions in living systems.

Methods

General methods. Unless otherwise noted, all commercial reagents and solvents were used without purification. Separation by flash column chromatography was performed on silica gel (200-300 mesh). ^{1}H and ^{13}C NMR spectra were recorded on Bruker AVANCE NEO 400 NMR spectrometer in $CDCl_3$ at 298K. Atmospheric pressure chemical ionization (APCI) mass spectra were recorded on a Thermo Scientific Q Exactive Focus (UltiMate 3000 HPLC) mass spectrometer. Single crystal X-ray diffraction data were collected at 100 K on a Rigaku-Oxford Diffraction SuperNova dual source diffractometer (Cu at Zero equipped with an AtlasS2 CCD using Cu Kα radiation). The data collected were processed by CrysAlisPro. The structures were solved by direct methods using Olex2 software, and the non-hydrogen atoms were refined anisotropically with SHELXL-2018 using a full-matrix least-squares procedure based on F^2. The weighted *R* factor, *wR* and goodness-of-fit *S* values were obtained based on F^2.The hydrogen atom positions were fixed geometrically at the calculated distances and allowed to ride on their parent atoms. Crystallographic data for the structures disclosed in this paper have been deposited at the Cambridge Crystallographic Data Center (CCDC).

NMR experiments. ^{1}H NMR experiments were performed on all of the host–guest pairs at a 1:1 ratio, and the peak shifts of the complexed host and guest relative to the free species were used to access complexation. *In the determination* of *binding constants* and *stoichiometries of complexes* ***G*⊠[P4-(OH)BPO]** (**G** = **1**–**41**), ^{1}H NMR titration[25] was performed in $CDCl_3$ with the host concentration of 10.0 mM and varying concentrations of the guest at 298K. By a non-linear curve-fitting method, the association constant between guest and host was calculated from the equation:

$$\Delta\delta = (\Delta\delta_\infty/[\text{host}]_0)\,(0.5[\text{guest}]_0 + 0.5([\text{host}]_0+1/Ka) - (0.5\,([\text{guest}]_0^2+(2[\text{guest}]_0(1/Ka-[\text{host}]_0)) + (1/Ka + [\text{host}]_0)^2)^{0.5}))$$

where Δδ is the chemical shift change of H_a on host at $[guest]_0$, $\Delta\delta_\infty$ is the chemical shift change of H_a when host is completely complexed, $[host]_0$ is the fixed initial concentration of host, and $[guest]_0$ is the varying concentrations of guest.

Calculations. Quantum chemical calculations were performed using Gaussian 16[32]. Fragment library compounds and designed “drug molecules” were calculated by RMO62X 6-311G (d,p) level of theory, and vibrational frequency calculations have be carried out to verify that all optimized geometries are true minima. Molecular volume (*V*) and surface area (*S*) of guest moleculars were calculated using Marching Tetrahedron algorithm via Multiwfn program[29]. Dipol momnetvalues were calculated using Gaussian 09 at the RB3LYP/6-31++G level of calcualtion.

Asphericity(Ω_a) was defined as

$$\Omega_a = \frac{(I_A - I_B)^2 + (I_A - I_C)^2 + (I_B - I_C)^2}{2(I_A + I_B + I_C)^2}$$

I_A, I_B and I_C are the principal moments of inertia of a molecule[28]. Mulliken charges were calculated by Gaussian 09 at PM6-D3 level. Molecular docking of **G⊂[P4-(OH)BPO]** (**G** = **39** or **40**) was performed with AutoDock Vina[48].

Declarations

Data availability

All data supporting the findings of this study are available within the article and its Supplementary Information files or from the corresponding authors upon reasonable request. Crystallographic data for the structures reported in this article have been deposited in the Cambridge Crystallographic Data Centre, under CCDC numbers: 2052256, 2052257, 2052258, 2052259, 2052260, 2052261, 2052262, 2052264 and 2052265. Copies of the data can be obtained free of charge from the CCDC via www.ccdc.cam.ac.uk/structures. All crystallographic data are available in supporting information.

Acknowledgements

This study was financially supported by National Key Research and Development Program of China (2017YFA0206500), National Natural Science Foundation of China (21871281 and 21902176), Shanghai Sailing Program (19YF1452900), Youth Innovation Promotion Association, CAS (2020291) and Science and Technology Commission of Shanghai Municipality (18DZ1100403). We thank the NMR Core Facility, School of Life Science and Technology, ShanghaiTech University for the assistance on NMR analyses.

Author contributions

Z.W., Y.A.L., W.-B.H., H.Y. and K.W. conceived the project. Z.W., T.C., H.L. and X.-L.Z. conducted the experiments and data analyses, including synthesis and characterization of **[P4-BPO(1-OH)]**, NMR experiments, crystal growths, quantum chemical calculations of the fragments, calculation of Mulliken charges, molecular docking, and single-crystal X-ray crystallographic analysis. Z.W., Y.A.L. and K.W. prepared the manuscript with contributions from all authors.

Competing interests

The authors declare no competing interests.

Additional information

Supplementary information is available for this paper at https://.....

Correspondence and requests for materials should be addressed to K.W.

Reprints and permissions information is available at www.nature.com/reprints.

References

1. Jarvis, L. M. The new drugs of 2019. *C&E News*. 98, 30-36 (2020).
2. Gao, M. & Skolnick, J. A Comprehensive survey of small-molecule binding pockets in proteins. *PLOS Comput. Biol.* ***9***, e1003302 (2013)
3. Stank, A., Kokh, D., B., Fuller, J. C. & Wade, R. C. Protein binding pocket dynamics. *Chem. Res*. **49**, 5, 809–815 (2016).
4. Zheng, X., Gan, L., Wang, E. & Wang, J. Pocket-based drug design: Exploring pocket space. *AAPS J*. **15**, 228–241 (2013).
5. Coleman, R. G. & Sharp, K. A. Protein pockets: Inventory, shape, and comparison. J. Chem. Inf. Model. 50, 589–603 (2010).
6. Weskamp, N., Hullermeier, E. & Klebe, G. Merging chemical and biological space: Structural mapping of enzyme binding pocket space. *Proteins: Struct., Funct., Bioinf.* **76**, 317–330 (2009).
7. McFedries, A., Schwaid, A. & Saghatelian, A. Methods for the elucidation of protein-small molecule interactions. *Biol.* **20**, 667–673 (2013).
8. Smith, B. D. (Ed.) *Synthetic Receptors for Biomolecules: Design Principles and Applications* (The Royal Society of Chemistry, Cambridge, 2015)
9. Erlanson, D. A. & Jahnke W. () *Fragment-based Drug Discovery*. *Lessons and Outlook* (Wiley-VCH, Weinheim, Germany, 2016).
10. Giordanetto, F., Jin, C.; Willmore, L., Feher, M. & Shaw, D. E. Fragment hits: What do they look like and how do they bind? *Med. Chem.* **62**, 3381–3394 (2019).
11. Sara M. Butterfield. S. M. & Rebek. J. A synthetic mimic of protein inner space: Buried polar interactions in a deep water-soluble host. *Am. Chem. Soc.* **128**, 15366-15367 (2006).
12. Tromans, R.A. et al. A biomimetic receptor for glucose. *Nature Chem.* **11**, 52–56 (2019).
13. Peñuelas-Haro, G. & Ballester, P. Efficient hydrogen bonding recognition in water using aryl-extended calix[4]pyrrole receptors. *Chem. Sci.* **10**, 2413–2423 (2019).
14. Kim, K. M. et al. Template-directed quantitative one-pot synthesis of homochiral helical receptors enabling enantioselective binding. *Chem. Int. Ed*. **59**, 22475-22479 (2020).

15. Chandramouli, N. et al. Iterative design of a helically folded aromatic oligoamide sequence for the selective encapsulation of fructose. *Nature Chem* **7,** 334–341 (2015).
16. Yao, H. et al. Molecular recognition of hydrophilic molecules in water by combining the hydrophobic effect with hydrogen bonding. *Am. Chem. Soc.* **140,** 13466–13477 (2018).
17. Huang, G., Valkonen, A., Rissanen, K. & Jiang, W. *endo*-Functionalized molecular tubes: Selective encapsulation of neutral molecules in non-polar media. *Chem Commun.* **52**, 9078–81 (2016).
18. Ma, Y.-L. et al. Biomimetic recognition of organic drug molecules in water by amide naphthotubes. *CCS Chem.* 2020, **2**, 1078–1092 (2020).
19. Ogoshi, T., Kanai, S., Fujinami, S., Yamagishi, T. & Nakamoto, Y. *para*-Bridged symmetrical pillar[5]arenes: Their Lewis acid catalyzed synthesis and host–guest property. *Am. Chem. Soc*. **130**, 5022-5023 (2008).
20. Xue, M., Yang, Y., Chi, X., Zhang, Z. & Huang, F. Pillararenes, A new class of macrocycles for supramolecular chemistry. *Chem. Res*. **45**, 1294-1308 (2012).
21. Song, N. & Yang, Y.-W. Applications of pillarenes, an emerging class of synthetic macrocycles. *China Chem*. **57**, 1185-11989 (2014).
22. Hu, X.-B., Chen, Z., Tang, G., Hou, J.-L. & Li, Z.-T. Single-molecular artificial transmembrane water channels. *Am. Chem. Soc.* **134**, 8384–8387 (2012).
23. Xie, C.-D. et al. Synthesis of pillar[n]arene[5-n]quinines via partial oxidation of pillar[5]arene. *J. Chem.* **33**, 379-383 (2015).
24. Pall, T. Determining association constants from titration experiments in supramolecular chemistry *Soc. Rev.* **40**, 1305–1323 (2011).
25. Wendler, K., Thar, J., Zahn, S. & Kirchner, B. Estimating the hydrogen bond energy. *Phys. Chem.* **114**, 9529–9536 (2010).
26. Jeffrey, G.-A. *An introduction to hydrogen bonding* (Oxford university, New York, 1997).
27. Smulders, M. M. J., Zarra, S. & Nitschke, J. R. Quantitative understanding of guest binding enables the design of complex host–guest behavior. *Am. Chem. Soc.* **135**, 7039–7046 (2013).
28. Lu, T. & Chen, F. Multiwfn: a multifunctional wavefunction analyzer. *Comput. Chem*. 33, 580–592 (2012).
29. Rumble, J. R., Lide, D. R. & Bruno, T. J. *CRC Handbook of Chemistry and Physics, 100th ed*. (CRC Press, Boca Raton, 2019).
30. https://scifinder.cas.org/scifinder/view/scifinder/scifinderExplore.jsf (accessed Dec 6, 2020).
31. Frisch M. J. *et al.Gaussian 16 Revision A 03* (Gaussian Inc., Wallingford, 2016)
32. Spencer, J.-N., Wolbach, W.-S., Hovick, J.-W., Ansel, L. & Modarress, K. J. Hydrogen bonding by alcohols and amines, *Solution Chem.* **14**, 805–814 (1985).
33. Mazur, K., Bonn, M. & Hunger, J. Hydrogen bond dynamics in primary alcohols: A femtosecond infrared study. *Phys. Chem. B* **119**, 1558–1566 (2015).

34. Lommerse, J. P. M., Price, S. L. & Taylor, R. Hydrogen bonding of carbonyl, ether, and ester oxygen atoms with alkanol hydroxyl groups, *Comput. Chem.* **18**, 757–774 (1997).
35. The typical length of a hydrogen bond in water is 97 Å (197 pm). Bond distances (measured from the hydrogen atom) range from 1.5 to 2.6 Å, or from 2.4 to 3.5 Å separate the two nonhydrogen atoms in a hydrogen bond. See Berg, J. M., Tymoczko J. L. & Stryer, L. *Biochemistry. 5th ed.* (Freeman. W. H. Press, New York, 2002).
36. Comer, J. E. A. Ionization constants and ionization profiles. In *Comprehensive Medicinal Chemistry II* Testa, B. & van de Waterbeemd, H. eds. (Elsevier Press, Amsterdam, 2007).
37. Habermann, S. M. & Murphy, K. P. Energetics of hydrogen bonding in proteins: A model compound study. *Protein Sci.* **5**, 1229–1239 (1996).
38. Chema, D., Eren, D., Yayon, A., Goldblum, A. & Zaliani, A. Identifying the binding mode of a molecular scaffold. *Comput. Aided Mol. Des.* **18**, 23–40 (2004).
39. Motiejunas, D. & Wade, R. C. Structural, energetic, and dynamic aspects of ligand-receptor interactions. In *Comprehensive Medicinal Chemistry II, Vol **4*** Mason, J. S. (Ed.) (Press, Amsterdam, 2007).
40. Naïm, M. et al. Solvated interaction energy (SIE) for scoring protein–ligand binding affinities. 1. Exploring the parameter space. *Chem. Inf. Model.* **47**, 122–133 (2007).
41. Baumann, M., Baxendale, I. R., Ley, S. V. & Nikbin, N. An overview of the key routes to the best selling 5-membered ring heterocyclic pharmaceuticals. *Beilstein J. Org. Chem.* **7**, 442–495 (2011).
42. Dalvie, D. K. et al. Biotransformation reactions of five-membered aromatic heterocyclic rings. *Res. Toxicol*. **15**, 269–299 (2002).
43. Surur, A. S., Schulig, L. & Link, A. Interconnection of sulfides and sulfoxides in medicinal chemistry, *Pharm.* **352**, 1800248 (2019).
44. Pacak, P. Polarizability and molecular radius of dimethylsulfoxide and dimethylformamide from refractive index data. *Solution Chem.*, **16**, 71–77 (1987).
45. Nepali, K., Lee, H. Y. & Liou, J. P. Nitro-group-containing drugs. *Med. Chem.* **62**, 2851–2893 (2019).
46. Fleming, F. F., Yao, L. H., Ravikumar, P. C., Funk, L. & Shook, B.C. Nitrile-containing pharmaceuticals: Efficacious roles of the nitrile pharmacophore. *Med. Chem.* **53**, 7902–7917 (2010).
47. Delost, M. D., Smith, D. T., Anderson, B. J. & Njardarson, J. T. From oxiranes to oligomers: Architectures of U.S. FDA approved pharmaceuticals containing oxygen heterocycles. *Med. Chem.* **61**, 10996–11020 (2018).
48. Trott, O. & Olson, A. J. AutoDock Vina: Improving the speed and accuracy of docking with a new scoring function, efficient optimization, and multithreading. *Comput. Chem*. **31**, 455–461 (2010).
49. Hammes, G. G., Chang, Y. C. & Oas, T. G. Conformational selection or induced fit: A flux description of reaction mechanism. *PNAS*. **106**, 13737–13741 (2009).
50. Vogt, A. D. & Di Cera, E. Conformational selection or induced Fit? A critical appraisal of the kinetic mechanism. *Biochemistry* **51**, 5894–5902 (2012).

Figures

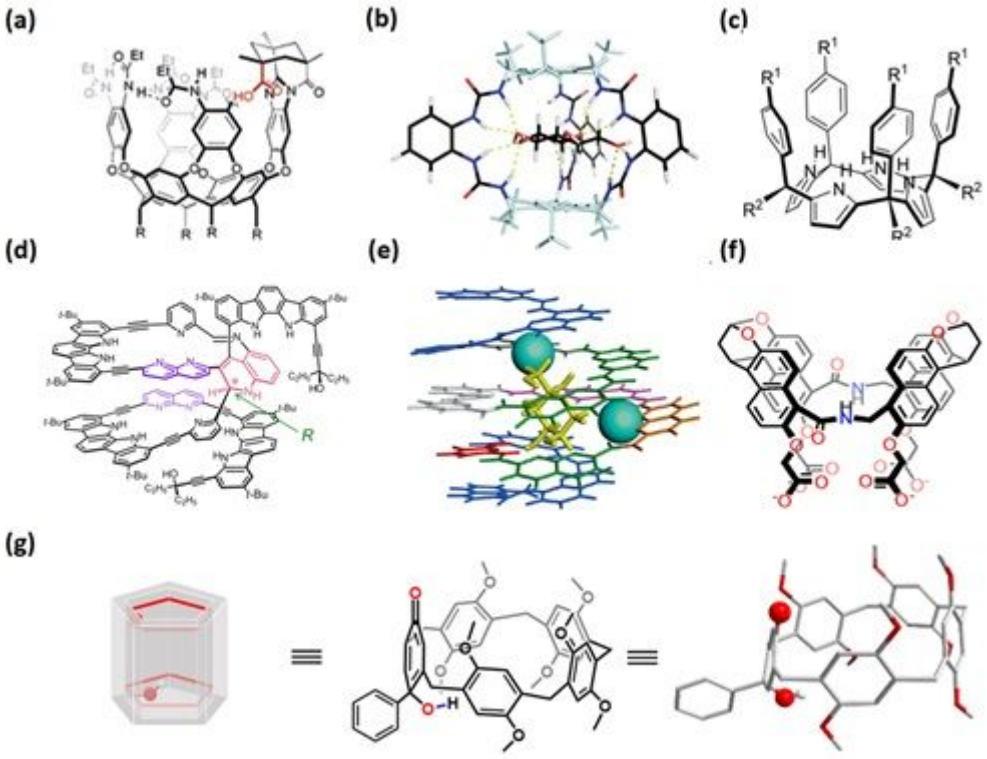

Figure 1

Biomimetic receptors. a, Chemical structure of cavitand11. b, Model of glucose receptor 212. c, Chemical structure of aryl-extended calix[4]pyrrole13. d, One-handed helical receptor P214. e, Crystal structures of capsule P-5 (with β-2C5-D-fructopyranose)15. f, Chemical structure of NT-syn16-18. g, Model, chemical and crystal structures of endo-[P4-(OH)BPO].

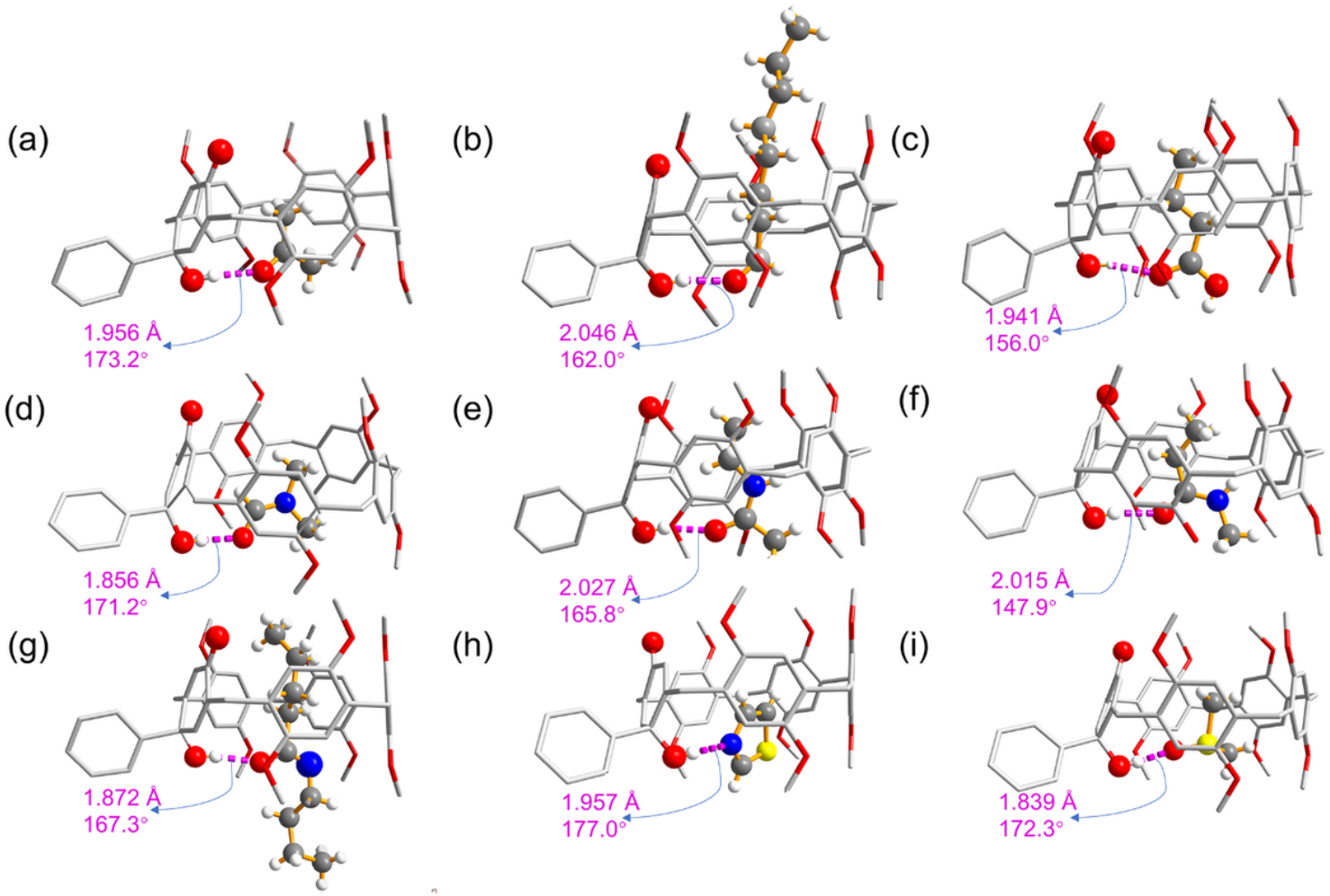

Figure 2

Crystal structures of fragment-pocket complexes G⊂endo-[P4-(OH)BPO]. a, G = acetone; b, G = 9; c, G = 13; d, G = 17; e, G = 21; f, G = 24; g, G = 25; h, G = 31; i, G = 35.

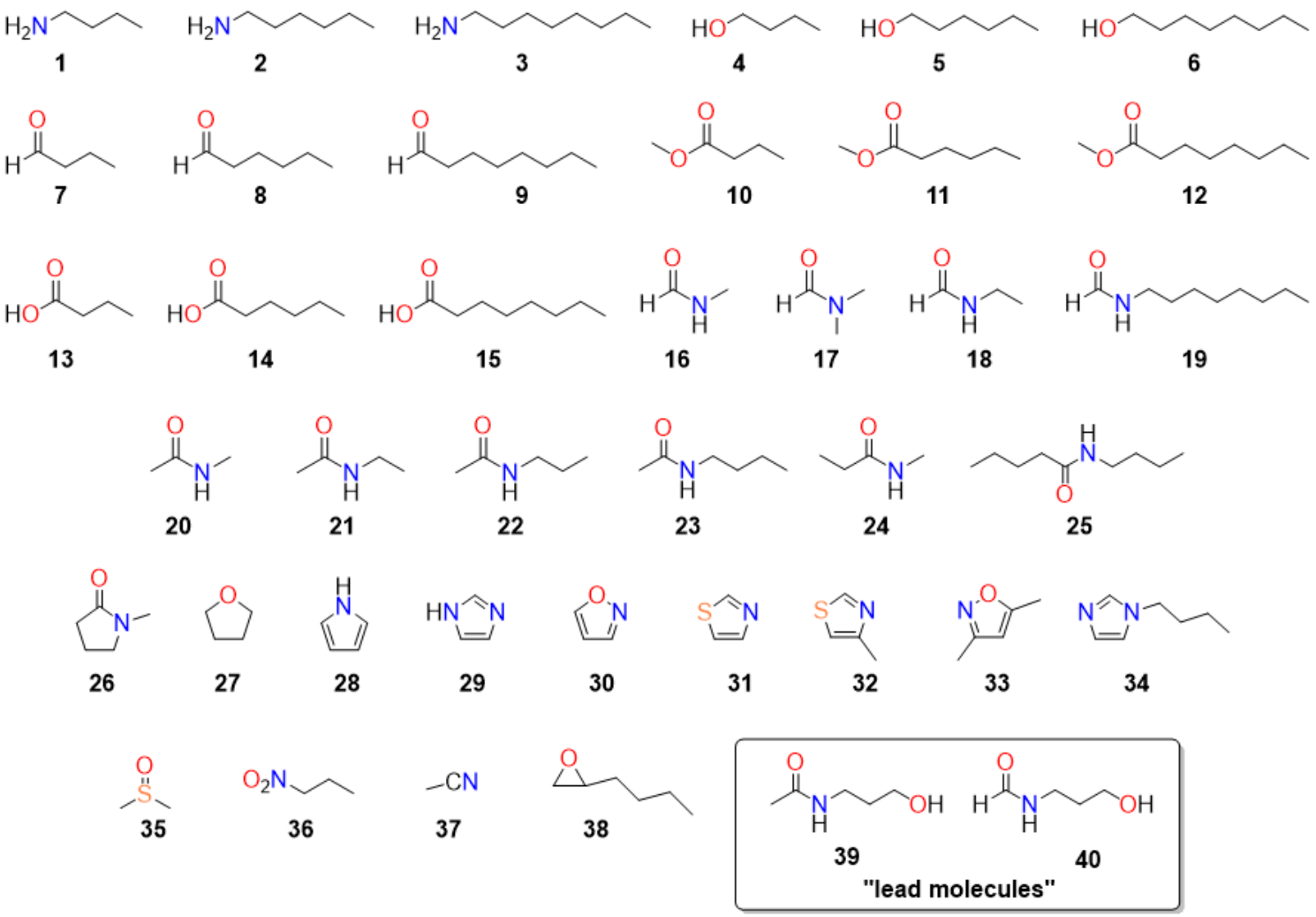

Figure 3

Structures of fragment library compounds and the designed “lead molecules”.

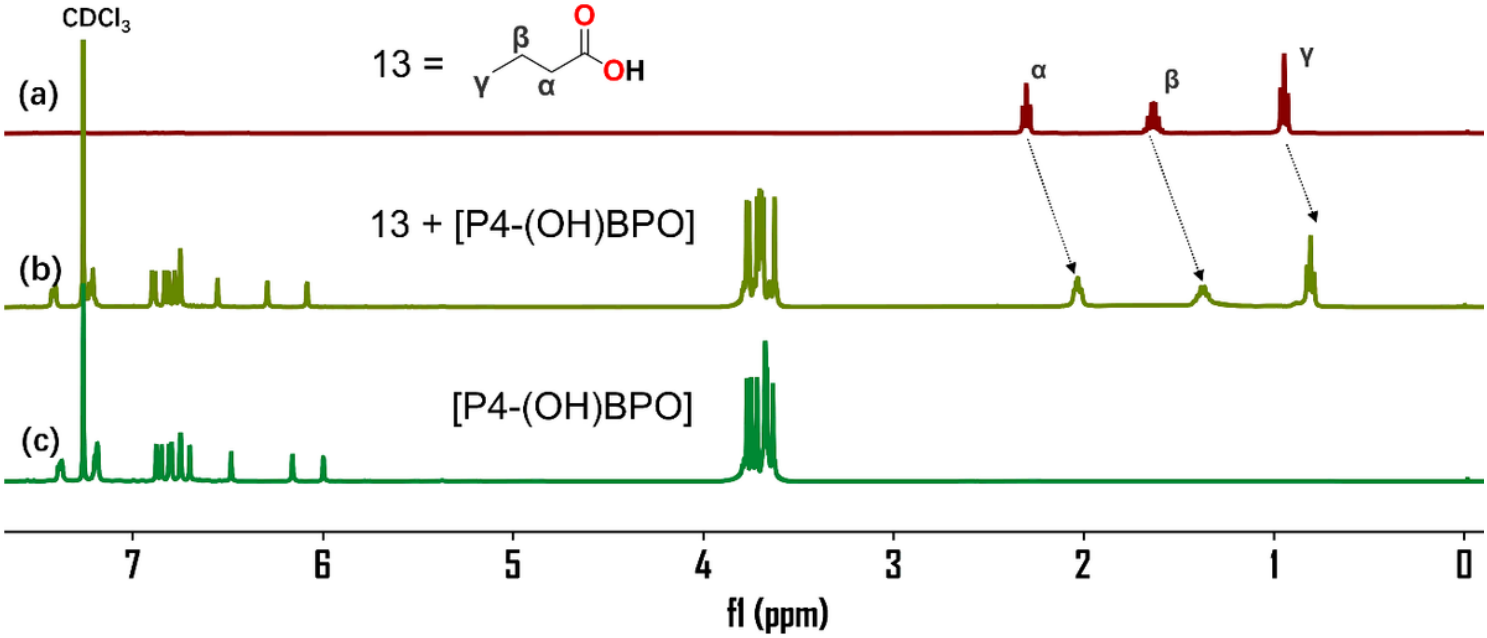

Figure 4

1H NMR (400 MHz, CDCl3) of [P4-(OH)BPO], 13 and complex 13⊂endo-[P4-(OH)BPO] (12.5 mM).

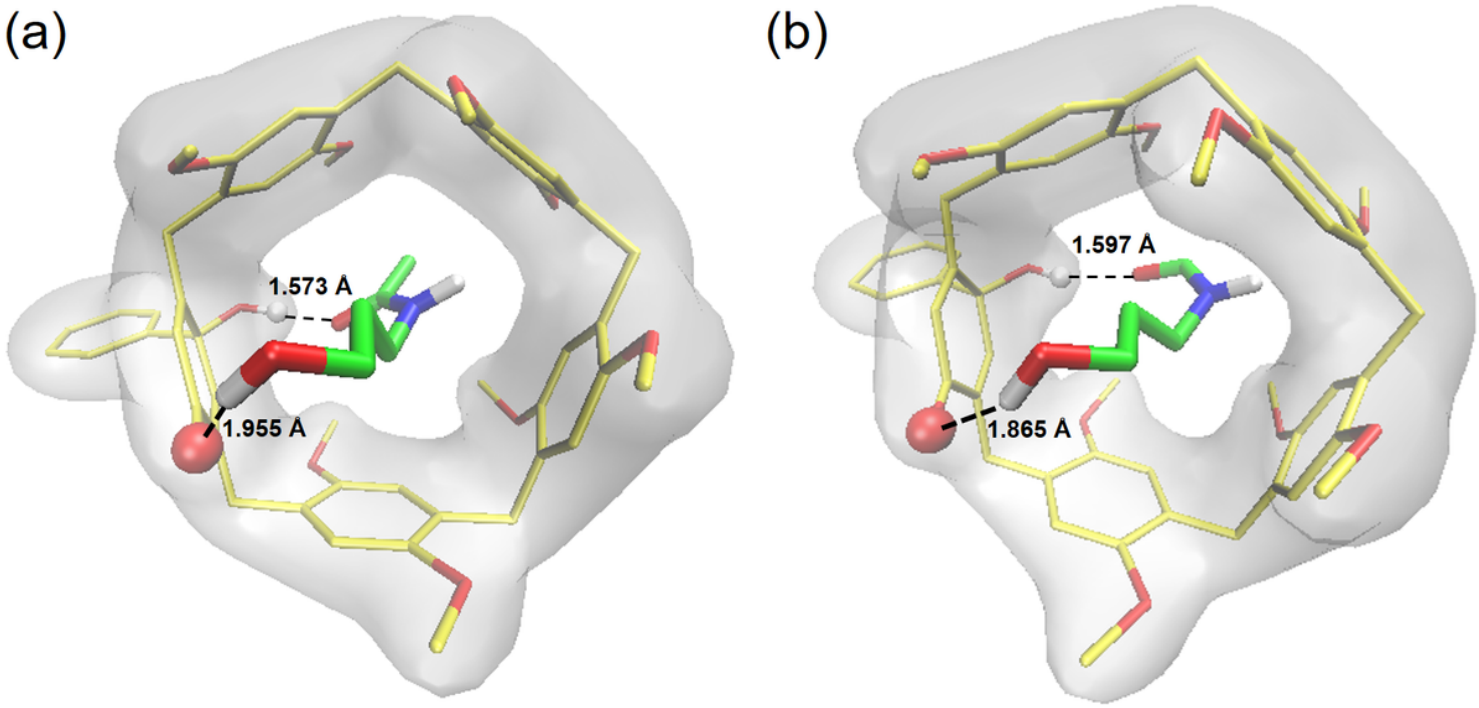

Figure 5

Molecular docking models of 39⊂endo-[P4-(OH)BPO] (a) and 40⊂endo-[P4-(OH)BPO] (b). 39 or 40 was docked into endo-[P4-(OH)BPO] with AutoDock Vina.48

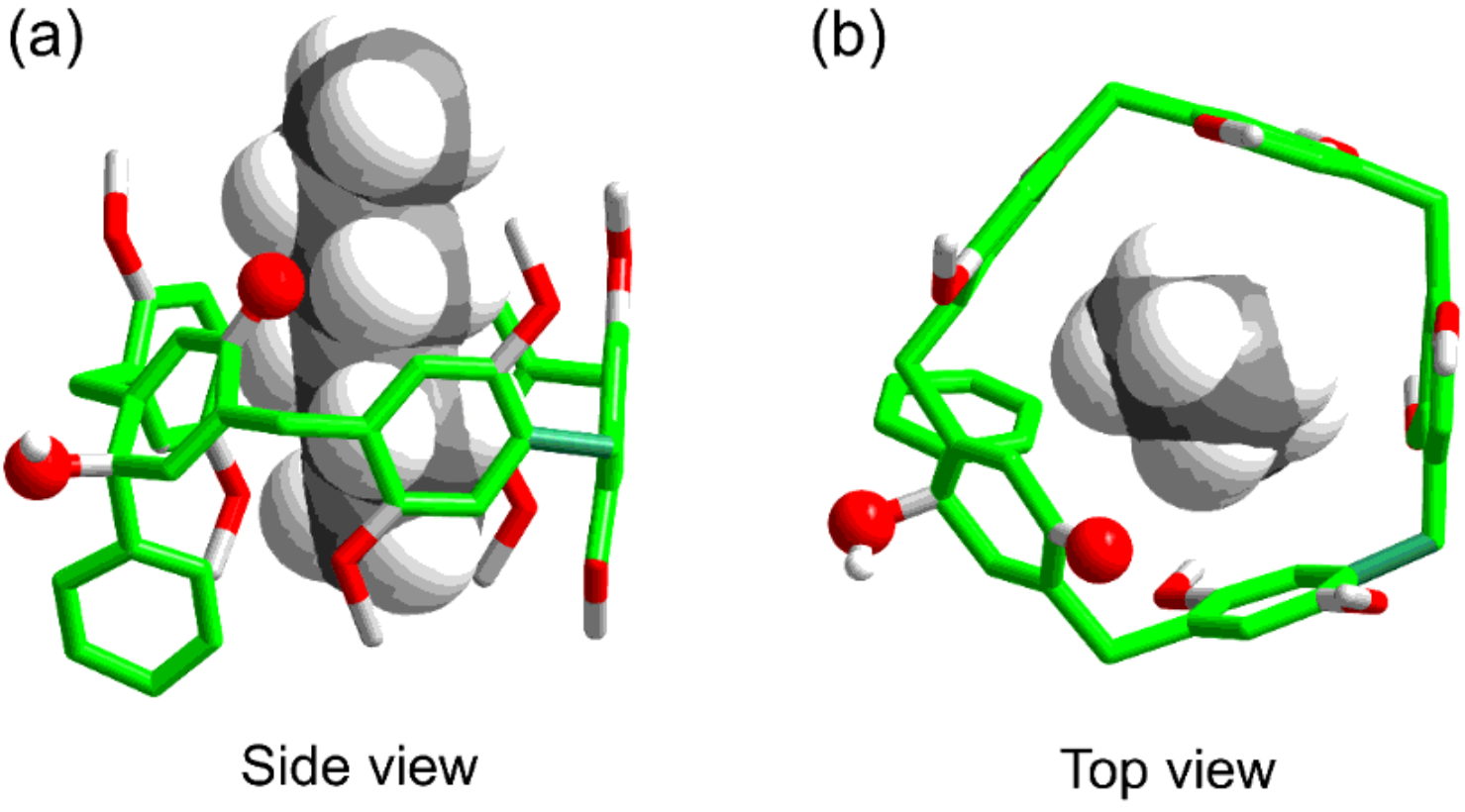

Figure 6

Crystal structure of hexane⊂exo-[P4-(OH)BPO].

Supplementary Files

This is a list of supplementary files associated with this preprint. Click to download.

- Supportinginformation.pdf
- GraphicalAbstract.jpg